SOME RESEARCH RELATED TO THE STRUCTURAL DYNAMICS OF LAUNCH VEHICLES

By Harry L. Runyan

NASA Langley Research Center
Langley Station, Hampton, Va., U.S.A.

Presented at the Sixth International Symposium on
Space Technology and Science

Tokyo, Japan
November 29 - December 4, 1965

SOME RESEARCH RELATED TO THE STRUCTURAL DYNAMICS OF LAUNCH VEHICLES

By Harry L. Runyan

NASA Langley Research Center

1584 7

SUMMARY

This paper treats recent advances in the use of dynamic models for structural dynamics and aeroelastic structures. Specifically, model tests of the Saturn I are discussed as well as tests of the 1/10- and 1/40-scaled models of the Saturn V. The problem of the effect of ground winds on launch vehicles is discussed, including a description of the model program and the results of some tests.

Also, the problem of the high-frequency buffet response of a launch vehicle adapter is treated, including a comparison of flight measurement with calculations.

Author

INTRODUCTION

The purpose of this presentation is to concentrate on structural dynamics and loads which are of importance in the design and operation of launch vehicles from the time of lift-off to the time at which the vehicle leaves the sensible atmosphere. This time interval is relatively short, being of the order of just several minutes.

What are some of the problems which are of concern to the dynamicist in designing and operating a launch vehicle? A listing of these problem areas is given in figure 1. On top of the figure is shown "input" loading, which is imposed on a "system" - the launch vehicle, and the "output" load, in terms of stresses and acceleration.

Buffet and acoustic loads are closely related as can be seen by the general similarity of the outputs. Winds, both ground and aloft, can induce bending moments which can involve such severe loads that certain portions of the vehicle must be designed to accommodate these loads.

Fuel slosh in general is a control problem; however, loads can be induced into the vehicle if the liquid oscillations are not kept to a minimum. Control loads during programed maneuvers are sometimes severe and, in particular, excessive loads from maneuvers should not be applied during periods of high loading from other sources. Recently, response and loads in the longitudinal direction have become of increasing concern. Since 90 percent of the weight of a typical liquid-propellant vehicle may be liquid, the coupling of the liquid system with the structure and engine is possible. During lift-off, when the hold-down clamps are released, a large dynamic response is found and is the

principal design consideration for the bottom of the tanks. Another dynamic phenomenon which has recently been found on two large vehicles is the coupling of the engine, turbopump, structure, and fluid components into a system that can be unstable. This has been referred to as the POGO problem, since the vehicle responds in a longitudinal direction, in the manner of a boy who is bouncing on a pogo stick.

One of the unfortunate aspects of this loading picture is the simultaneity of the occurrence of some of these loads. In figure 2, a plot of various loading sources against time of flights is shown, where the black area indicates the probable time at which the particular event will occur. The point here is that it appears rather black between the transonic region and the maximum dynamic pressure region for most of the loading conditions. These combined loads present a rather complex interaction problem which, at the present time, is not entirely understood.

To illustrate this loading picture in more detail, on figure 3 is plotted bending moment versus vehicle station. The curve labeled "capability" represents the bending-moment capability remaining after such known loading factors as internal pressure, acceleration, and drag have been accounted for. Thus, the loads from the remaining sources can be summed to ensure that their total does not exceed the capability curve. Of particular note is the large increment in bending moment due to winds aloft. At certain times the winds may be very severe, and may be as high as 100 meters per second or, in rare instances, even higher.

To illustrate this wind picture lines of constant wind velocities for the Northern Hemisphere are presented (isotacks) as obtained from reference 1. A typical result is shown in figure 4. This figure represents the average wind over a 3-month period for an altitude of 11.8 km. Statistically, these velocities will be exceeded only 1 percent of the time. Note the low wind velocity found both on the Equator and in the Arctic region. Of particular interest, however, since this meeting was held in Tokyo under the auspices of the Japanese Rocket Society, is the high wind region over Japan. The 99 percent wind velocity is about 90 meters per second, which is the highest wind speed of any area in the Northern Hemisphere.

DYNAMIC MODELING

A basic ingredient in the solution of most structural dynamic problems is a knowledge of the vibration modes. For complex cases, theory is not adequate and the use of dynamic models is mandatory. The next section of the paper will be concerned with specific examples of dynamic model testing, concentrating on the problem of the gross vehicle vibratory motion.

1/5-Scale Vibration Model of Saturn

Description.- The 1/5-scale Saturn model described in reference 2 was constructed for the study of lateral bending vibrations; therefore, the important parameters to be scaled were the mass-stiffness ratios. Such parts as aerodynamic fairing and fuel piping were not scaled since they did not contribute to stiffness; however, lead ballast weights were used to simulate their mass. Furthermore, the vibrations of principal interest were the overall vehicle modes, so local panel stiffnesses were not scaled. Other factors, such as fuel sloshing, were considered to have a secondary effect on the overall vehicle vibration and so were not scaled. The model is shown on the left in figure 5, and the full-scale vehicle is shown on the right in a vibration test tower.

The type of scaling chosen for the Saturn model was a component-by-component uniform reduction of dimensions to 1/5 of the full-scale values, using the same materials as the full scale. This replica type of scaling was chosen because of the structural complexity of the Saturn booster with the resulting difficulty of determining accurate equivalent stiffness and mass properties for the multiple-beam truss-work assemblies incorporated in the vehicle.

Results.- Some results of the model vibration test are shown in figures 6 and 7. In figure 6, the first or fundamental mode shapes and frequencies of the model and full-scale vehicles are shown with the vehicle ballasted to simulate the maximum dynamic-pressure weight condition. This figure shows almost exact agreement between model resonant frequency, when adjusted by the scale factor, and the full-scale resonant frequency. The mode shapes of the full-scale vehicle and the model are in good agreement as can be seen from comparison of the circles with the square symbols. The booster outer tanks, which are free to deflect independently of the center tank except at their ends, are shown in this figure to have the same deflection as the center tank, and this mode has the appearance of the more conventional bending modes obtained from nonclustered vehicles.

In contrast, the second vibration mode, shown in figure 7, shows one of the unusual vibration modes associated with the clustered arrangement of the Saturn booster. There is about a 10-percent difference in frequency between model and full scale in this mode, and comparison of the circles with the squares shows fairly good agreement of model with full-scale mode shape. The typical outer tank indicated by the flagged symbols is seen to deflect in the opposite direction as the center tank. Cross section A-A at the midsection of the booster shows that when the center tank deflects upward as indicated by the arrow, the outer tanks are deflecting independently in the downward direction. This unusual mode shape where the outer tanks deflect in the opposite direction from the center tank is associated with the clustered arrangement of the booster tanks and has been termed a "cluster mode."

Saturn V Dynamic Models

Figure 8 illustrates the present modeling project, which is a 1/10-scale replica model of the Saturn V. The model is 36 feet high, including the Apollo payload. The model will duplicate all of these essential details up to the Apollo payload. The general type of construction of the full scale including skin stringer, waffle pattern, integrally milled stringer, and corrugated skin is being followed. As an example of the construction detail adhered to in the model, figure 9 illustrates the interior of the first-stage tankage. Note in particular the detail in the fuel slosh baffles which are the thin corrugated rings located on the circumference of the tank. The three corrugated pipes are three of the five tunnels through which the fuel lines pass through the bottom tank to the five individual pumps for each engine.

In addition to the 1/10-scale model, a 1/40-scale model is being constructed, which is shown in figure 10 and which is about 9 feet high. The modeling concept for this case involved only the duplication of the mass and stiffnesses, and does not follow the replica concept.

A sampling of the results of vibration testing of the two scaled models along with theoretical predictions are given in figure 11 taken from reference 3. Here the lateral vibration frequencies for the first three modes are plotted as a function of the first-stage propellant load, with the upper stages remaining full. The experimental results are plotted as open symbols and the analytical results are shown as solid or dashed lines. Examination of the experimental data indicates excellent agreement between the two models, in spite of the fact that one model was essentially an exact replica of the full scale (1/10), whereas the other (1/40) was designed solely on the basis of an equivalent stiffness and mean distribution.

The analytical results are interesting from the standpoint of the pretest results. The pretest results were based on estimation of the stiffness and mass from early design drawings. The post-test results were obtained after the model had been constructed, parts weighted, and better and more detailed stiffness estimates made. The increase in accuracy of the analytical results is apparent, and may be considered acceptable for design purposes.

BUFFETING

The term "buffeting" is really not very well defined and precise. For the purposes of this paper, the term "buffet" will refer to aerodynamic flows involving departure from potential flow with consequent flow breakdown and separation which can result in structural response of the vehicle. Obviously, this is a rather broad definition and is symptomatic of the wide spectra of buffet problems.

The occurrence of buffeting on launch vehicles has been a surprise to many people; the long cylindrical shape of a typical launch vehicle did not appear at first to offer any substantial problem. However, certain vehicle

failures in the early days of the space program were diagnosed to have been due to possible flow breakdown, resulting in structural failure. (See ref. 4.)

As an illustration of the response of a structure to high-frequency buffet, some work is in progress on attempts to calculate the random response of a complex structure such as a launch-vehicle adapter for comparison with results measured in flight. For this example, the comparison of the calculated and measured response of the adapter used on an early Mercury flight will be shown. The adapter is a ring and stringer stiffened shell structure which connected the spacecraft to the launch vehicle. The Mercury had an abort escape tower containing a solid-propellant rocket projecting ahead of the spacecraft. The combination of the rocket, the open tower, and the shape of the Mercury capsule resulted in some rather severe buffeting loads on the adapter immediately below the capsule. Measurements of the acceleration response of a point on the adapter were made in flight, and efforts have since been made to estimate the response spectra. The following results were obtained under contract to NASA-Langley Research Center by the McDonnell Aircraft Corporation, and are reported in reference 5.

The fundamental equation for the cross-power spectral density is

$$S_w^{ab}(\pm\omega) = \left[\phi_{aI}\right]\left[S_q^{IJ}(\pm\omega)\right]\left[\phi_{bJ}\right]^T$$

where

$$S_q^{IJ}(\pm\omega) = \frac{1}{Z_I(\pm\omega)Z_J^*(\pm\omega)} \int_{x_1}^{x_2}\int_0^{2\pi}\int_{x_1}^{x_2}\int_0^{2\pi}\left[S_p(x,\theta,x',\theta',\pm\omega)\phi_I(x,\theta)\phi_J(x',\theta')r(x)r(x')d\theta\, dx\theta'\, dx'\right] \qquad (1)$$

where

ϕ_I, ϕ_J mode deflection shape in I,J vibration modes

x longitudinal coordinates

θ angular position

where

$$Z_I(\pm\omega) = M_I\omega_I^2\left[1 - \left(\frac{\omega}{\omega_I}\right)^2 + i2\zeta_I\left(\frac{\omega}{\omega_I}\right)\right]$$

$$Z_J^*(\pm\omega) = M_J\omega_J^2\left[1 - \left(\frac{\omega}{\omega_J}\right)^2 - i2\zeta_J\left(\frac{\omega}{\omega_J}\right)\right]$$

S_p is the cross-power spectrum of the pressures defined by the cross-correlated function

$$R_p(x,\theta,x',\theta',\tau) = \lim_{T \to \infty} \frac{1}{2T} \int_{-T}^{+T} p(x,\theta,t+\tau)p(x',\theta',t)dt \qquad (2)$$

where

$$S_p(x,\theta,x',\theta',\pm\omega) = \int_{-\infty}^{\infty} e^{-i\omega\tau} R_p(x,\theta,x',\theta',\tau)d\tau \qquad (3)$$

The basic and difficult problem is the accurate and practical integration of equation (1). There are two difficult quantities to determine. First, is the aerodynamic input characterized by the cross-spectra S_p. No analytical methods are available for its prediction in complex cases such as the Mercury configuration. For boundary-layer phenomena, estimates can be made based on many past experiments. For this case, however, resort must be made to measured quantities. The input pressure spectra were estimated from wind-tunnel measurements utilizing a 7-percent scaled rigid model of the Mercury-Atlas configuration including the escape tower. The vibration modes of the adapter were determined analytically, but the frequencies were adjusted to agree with results of ground vibration tests of a full-scale adapter. One of the significant factors in such an analysis is a good estimate of the structural damping, since the response is a direct function of the reciprocal of the structural damping at a resonant frequency. Damping is a very difficult and tenuous quantity to determine; many factors influence its value such as temperature, quality of joints, end condition, amplitude, etc. For this case, a nominal value of 2-percent critical damping was assumed. The integration required in equation (6) was accomplished by dividing the structure into 112 subareas, adjusting the properties across each subarea and proceeding with the necessary integrations as described in detail in reference 5.

The comparisons of flight and calculation are shown in the next two figures. In figure 12 is plotted the acceleration in g's rms (0 to 600 cps) versus Mach number of a point on the adapter. The curve represents the flight data; the points represent calculated data. The agreement is quite good considering the numerous approximations made in the analysis. Actually, what is being compared here is the total area under each acceleration spectrum at a given Mach number, since the area under a spectrum represents the mean square of the quantity. Information about the frequency content must be obtained from the spectrum itself.

In the next figure (fig. 13) is shown the acceleration spectrum in g^2/cps versus frequency in cycles per second for Mach number of unity. The dashed line is the result of the analysis, and the solid line is the value obtained from flight. Here the comparison is not as good as in the previous figure;

however, the results are still considered excellent. For instance, the magnitude of the peaks is very similar, and when one considers such important factors as the variability of structural damping, the effects of acceleration loads on the adapter as well as bending loads due to winds aloft, all of which were neglected in the analysis, the correlation is very good. Examination of the maximum response peaks indicates a shift in frequency. Four large peaks are apparent in each set of data with the analytical peaks occurring at a lower frequency.

Thus, the picture for the estimation of the random response of a complex structure seems to be brightening, providing such factors as structural damping, vibration mode shapes, and the random aerodynamic input are adequately and carefully determined.

RESPONSE TO GROUND WINDS

For a final topic, another case of structural response to random disturbances will be discussed, namely, the response of a launch vehicle (as it stands on its launch pad) to ground winds. This is really an age-old problem; civil engineers have been concerned with the oscillation of smokestacks, buildings, and suspension bridges for a number of years. In spite of all this background work, it is still not possible to analytically predict the motion of a structure to ground winds. For large launch vehicles, this is a problem which must be solved. These wind loads create problems in structural strength, guidance alinement, and clearance between adjacent structures. A more thorough discussion of this problem is given in reference 6.

In order to obtain immediate answers for engineering purposes, resort to the testing of dynamic models in wind tunnels and the measurement of the response is necessary. But before discussion of the program, what is the basic problem? In figure 14 are shown schematically a launch vehicle, a tower, and a wind profile. The wind profile (on the right) can be considered as a steady wind having a profile varying in the vertical height upon which may be superimposed turbulence. The wind may or may not pass near or through an adjacent launch tower before impinging on the vehicle, but the presence of the tower is vital in studying this problem. The steady-wind component may impose both static and dynamic loads on the vehicle. The static load response is primarily in the direction of the mean wind, and the dynamic response which is associated with vorticity shed from the vehicle is largest in the direction perpendicular to the wind. These dynamic loads, which may result from either a random forced response or a periodic self-excited response, may be several times larger than the static drag loads.

To provide an idea of the extent of the effort on ground winds, figure 15 shows nine different configurations which have been investigated in the Langley Research Center 16-Foot Transonic Dynamics Tunnel, ranging from a 15-percent-scale Scout vehicle to a 3-percent-scaled Saturn V. Full-scale Reynolds number is simulated for all vehicles except the 3-percent Saturn V which was tested at about one-third full-scale Reynolds number.

Some interesting results obtained on the 3-percent model of the Saturn V are shown in figure 16. The maximum lateral oscillatory bending moment is plotted against the Strouhal number U/fD, where U is the mean steady velocity, f is the fundamental bending frequency, and D is the diameter of the base.

The response is given for three values of damping. For the lowest damping case, a very large response was found over a very limited range of Strouhal number. As the damping was increased, this peak completely disappeared. It is believed that this peak response is a case of self-excited motion, as in flutter, whereas the response for the higher damping ratio is simply the response of a low damped system to random inputs. The typical response record is shown, the large peak response being of the nature of a pure sine wave at the fundamental frequency. The response for the two higher damping ratios appears as the response of a single-degree-of-freedom system to a random input. Research is continuing to better define this large response.

CONCLUDING REMARKS

The fundamental ingredient in the solution of structural dynamics problems is a knowledge of the vibration characteristics of the structure. A dynamic model program was described, which provides for input data for both direct design analysis as well as for correlation of theory and experiments. Two examples of problem areas were discussed in which the random nature of the input is an essential part of the problem. These were the buffet response of a localized area of a launch vehicle and the response of a vehicle to ground winds.

REFERENCES

1. Henry, R. M.; and Cochrane, J. A.: Geographical Variations of Wind Loads on Vertically Rising Vehicles. Journal of Applied Meteorology, Vol. 3, No. 6, December 1964, pp. 734-743.

2. Mixson, J. S.; Catherine, J. J.; and Arman, A.: Investigation of the Lateral Vibration Characteristics of a 1/5-Scale Model of Saturn SA-1. NASA TN D-1593, January 1963.

3. Leadbetter, S. A.; and Raney, J. P.: Analytical and Experimental Studies of the Dynamics of Launch Vehicles. AIAA Symposium on Structural Dynamics and Aeroelasticity, Boston, Mass., August 30 - September 1, 1965.

4. Rainey, A. G.: Progress on the Launch-Vehicle Buffeting Problem. Journal of Spacecraft and Rockets, May-June 1965.

5. Schweiker, J. W.; and Davis, R. E.: Response of Complex Shell Structures to Aerodynamic Noise. Contract NAS1-3179, by McDonnell Aircraft Corp., St. Louis, Mo.

6. Reed, W. H., III: Models for Obtaining Effects of Ground Winds on Space Vehicles Created on the Launch Pad. Conference on the Role of Simulation in Space Technology, Virginia Polytechnic Institute, Engineering Extension Series, Circular No. 4, Part C, August 17-21, 1964.

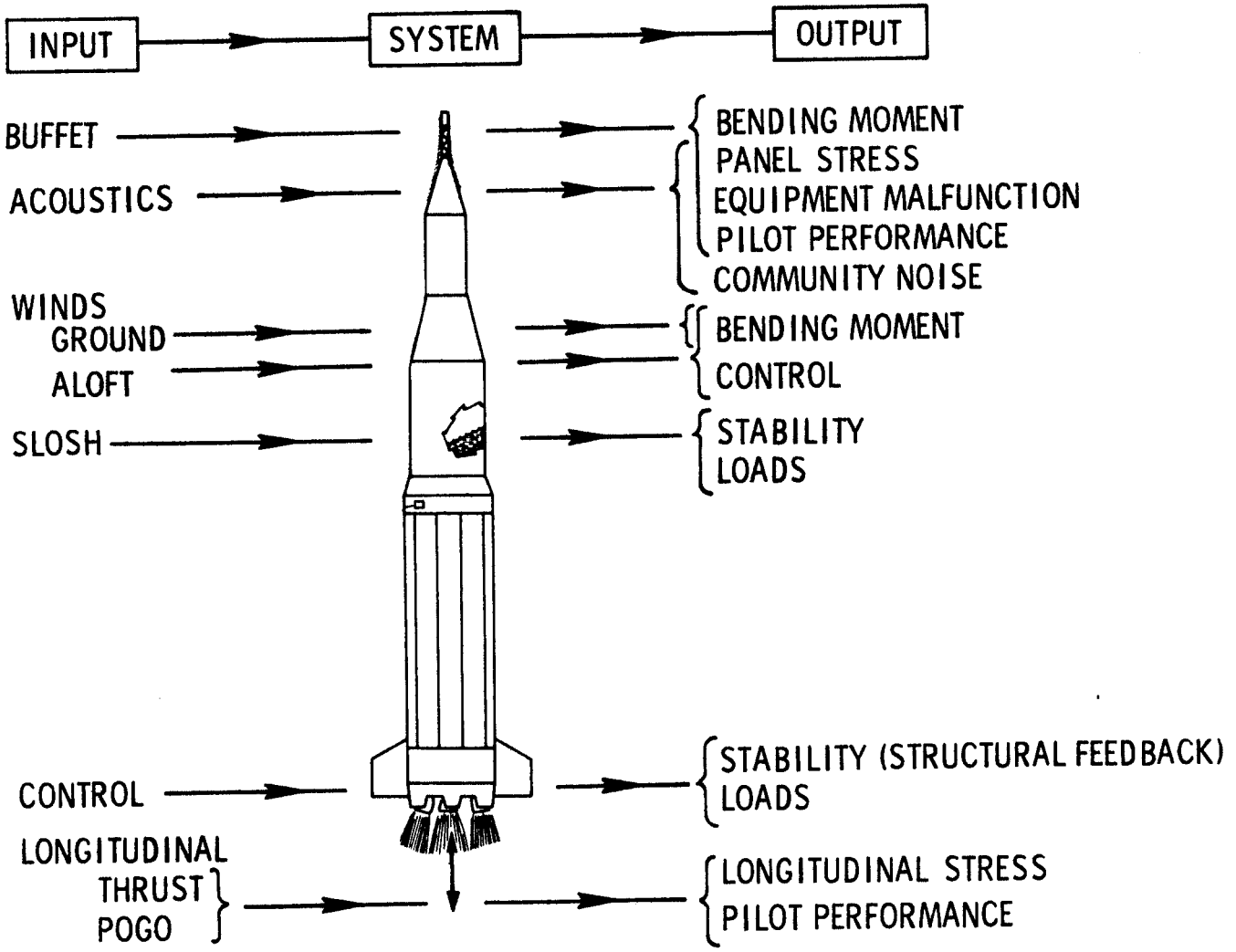

Figure 1.- Structural dynamic loading.

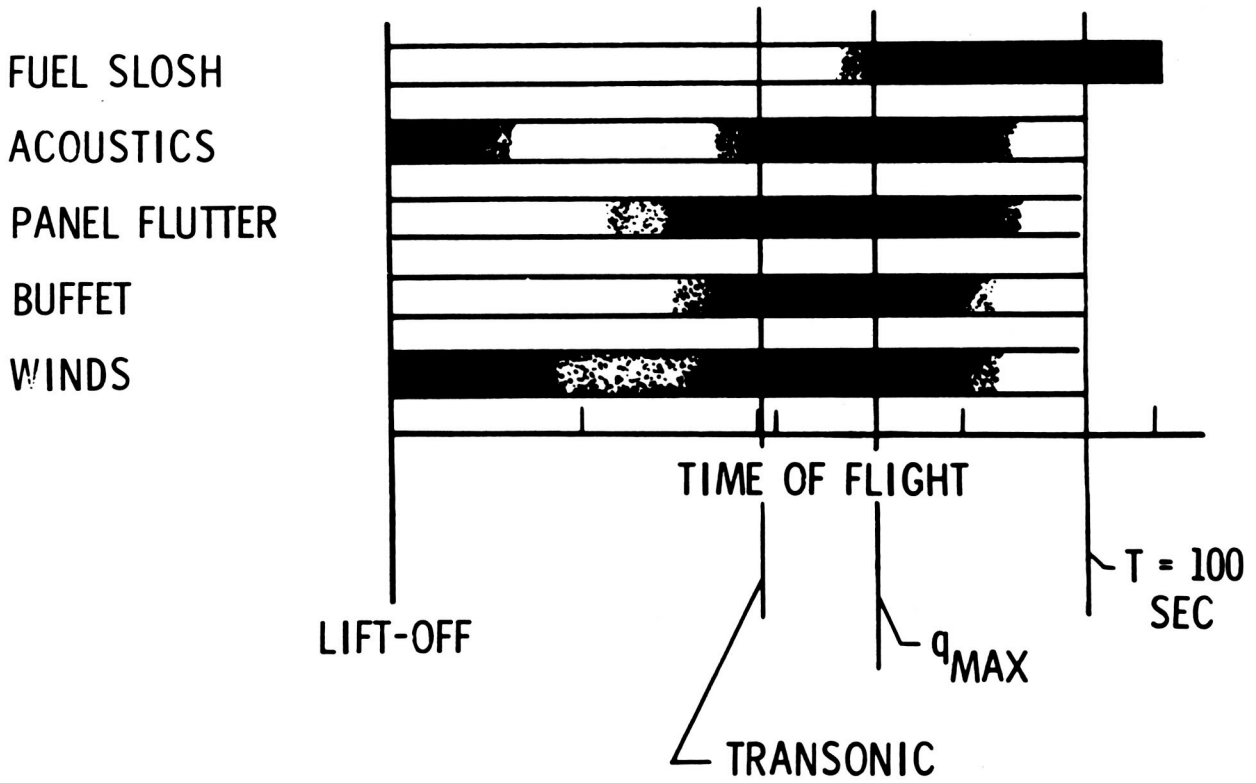

Figure 2.- Loading conditions versus time of flight.

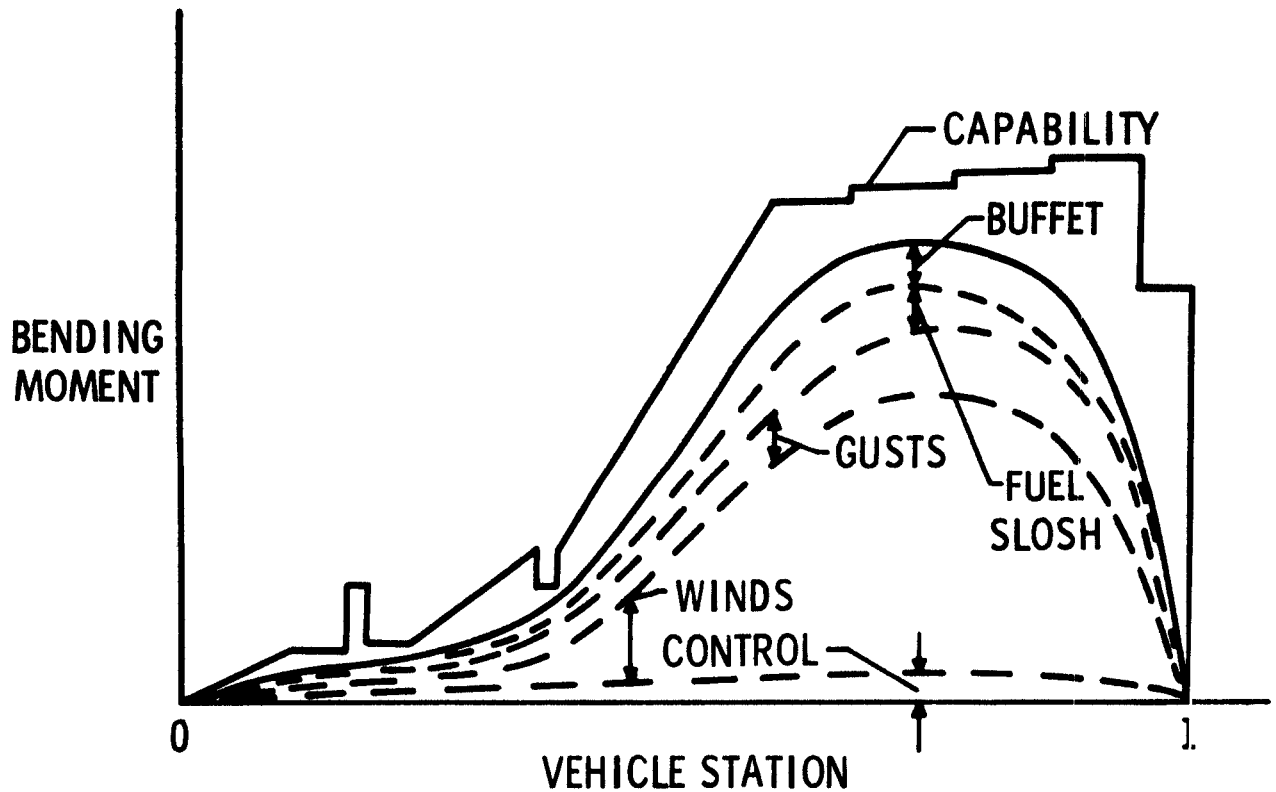

Figure 3.- Bending-moment capability and applied loads.

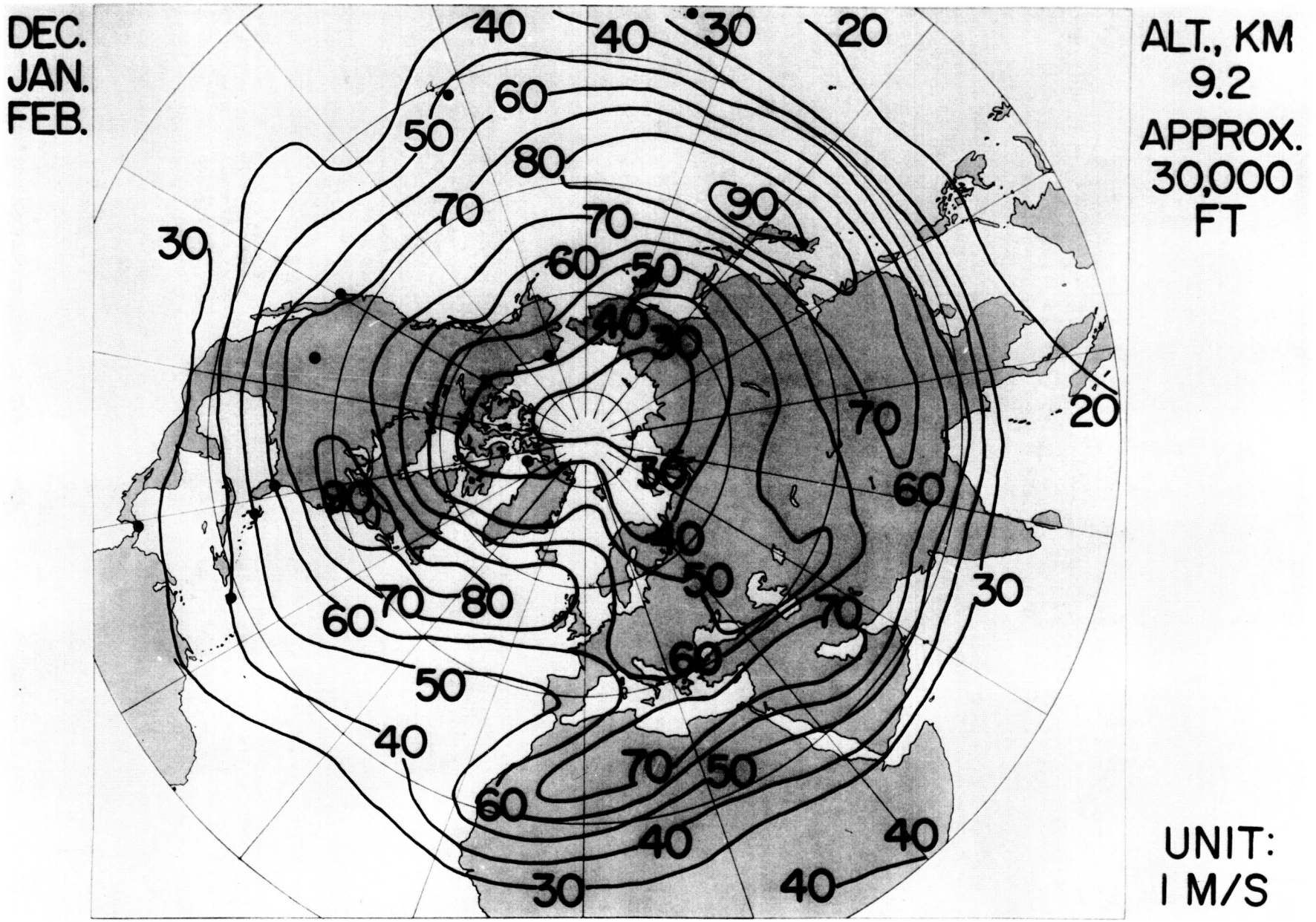

Figure 4.- 99 percent wind speed for Northern Hemisphere.

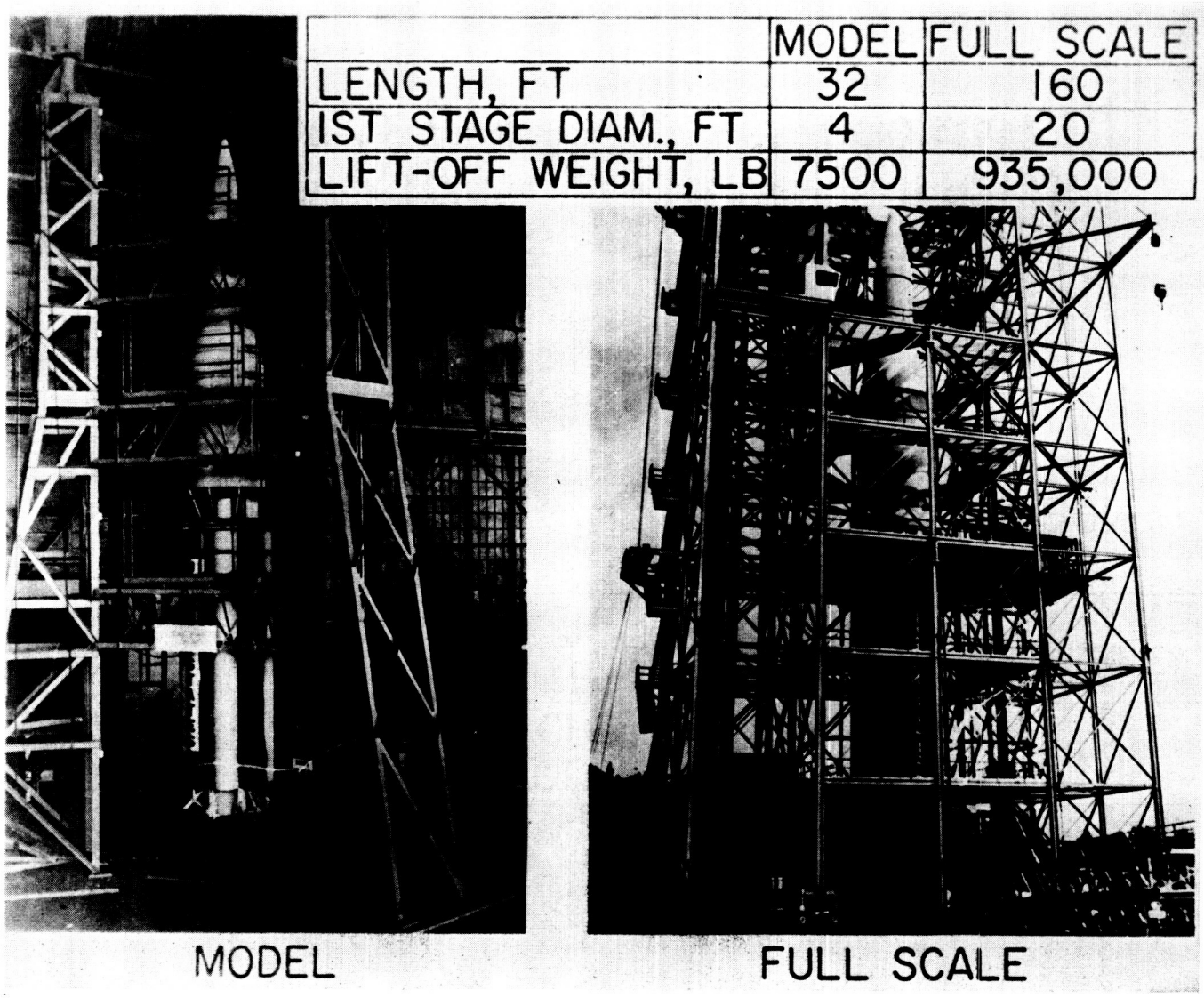

	MODEL	FULL SCALE
LENGTH, FT	32	160
IST STAGE DIAM., FT	4	20
LIFT-OFF WEIGHT, LB	7500	935,000

Figure 5.- Saturn vibration-test vehicles.

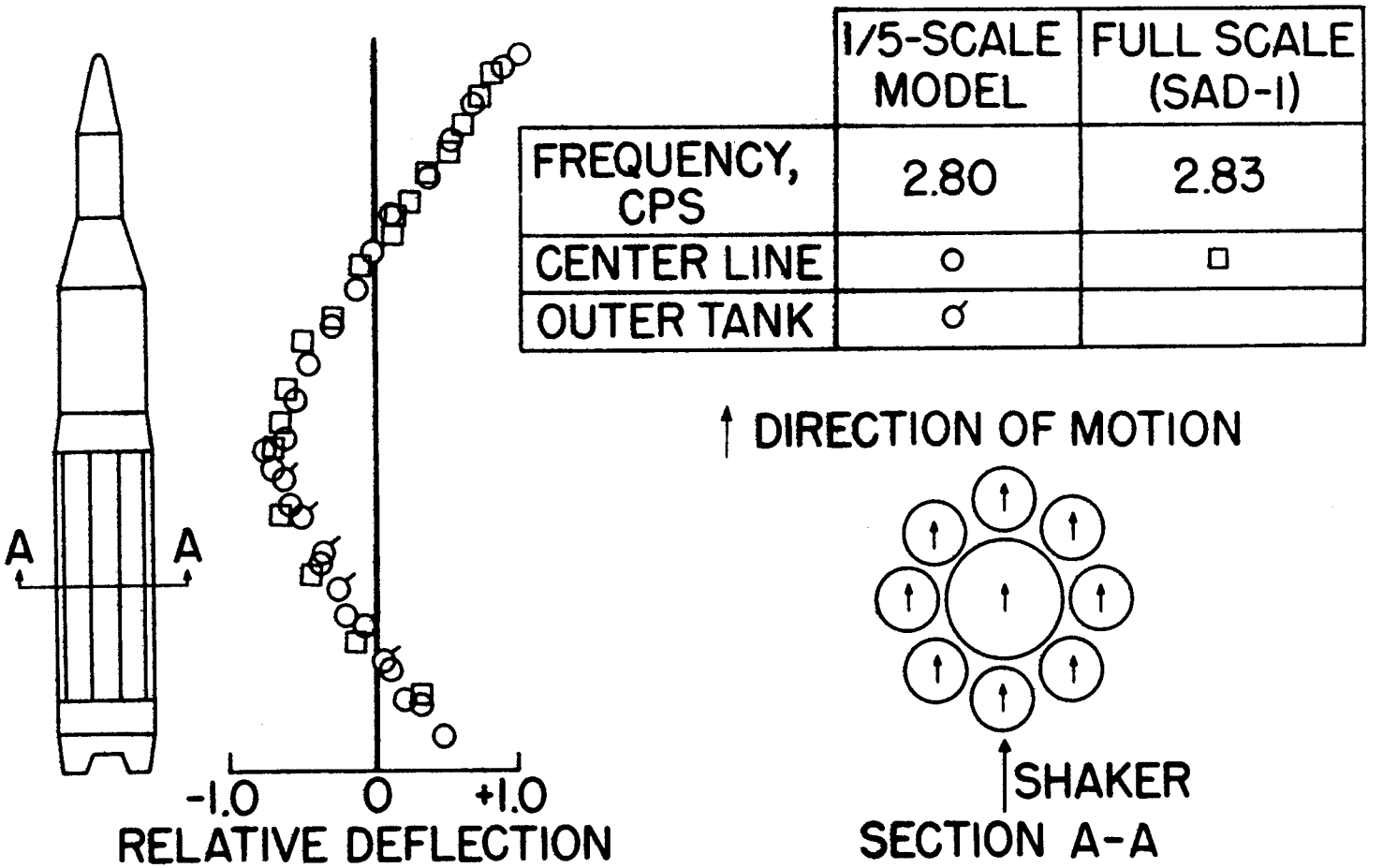

Figure 6.- First vibration mode at q_{max}.

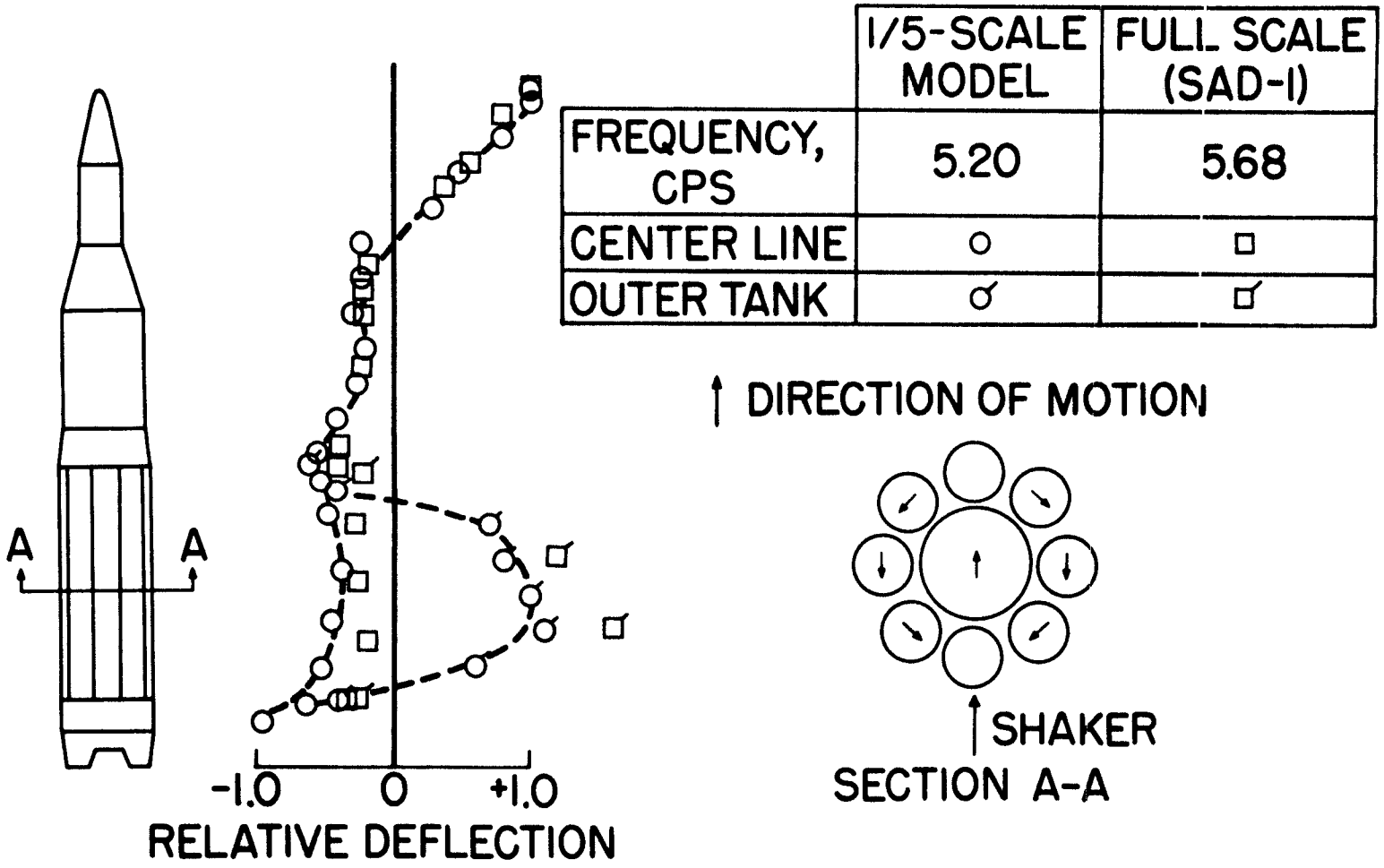

Figure 7.- Second vibration mode at q_{max}.

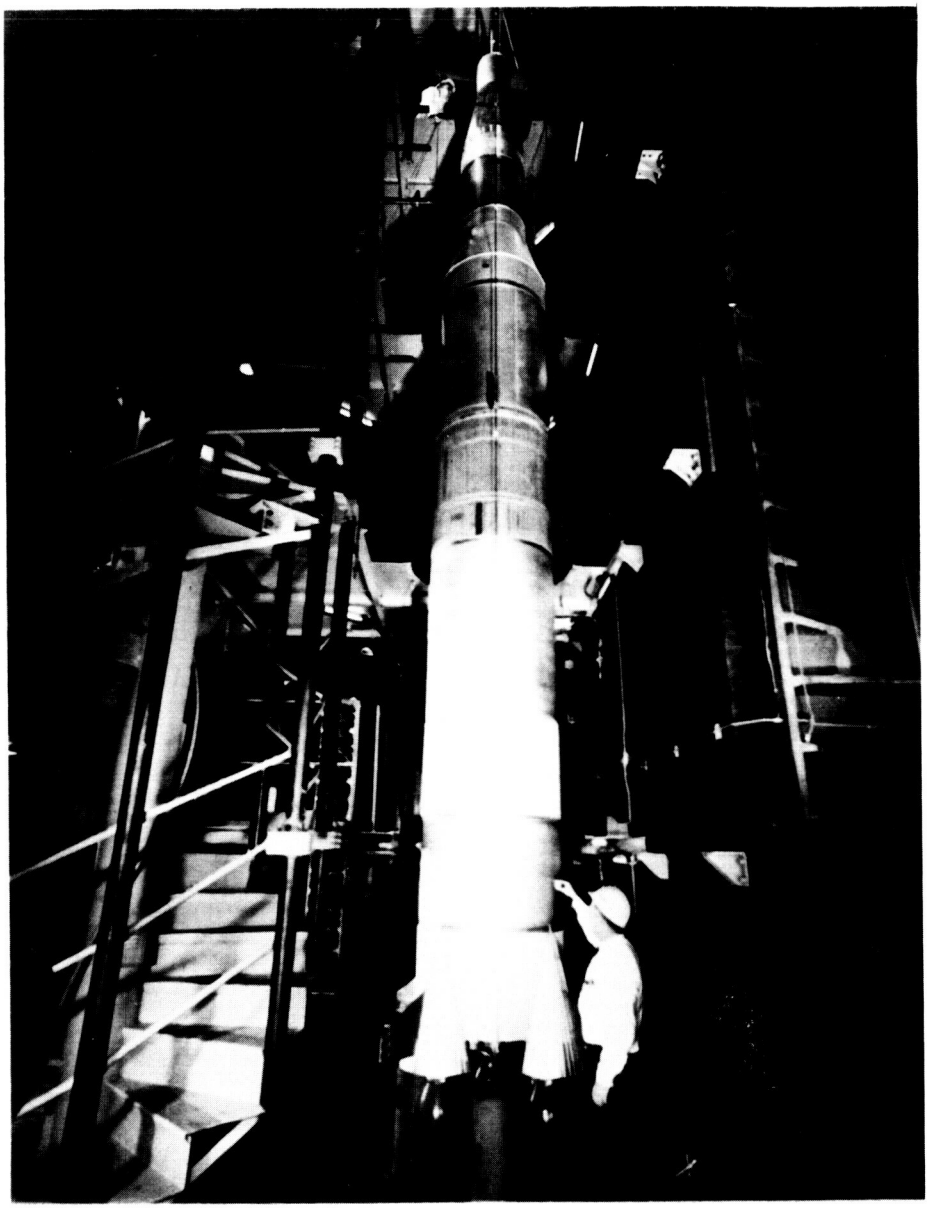

Figure 8.- 1/10-scale model of Saturn V.

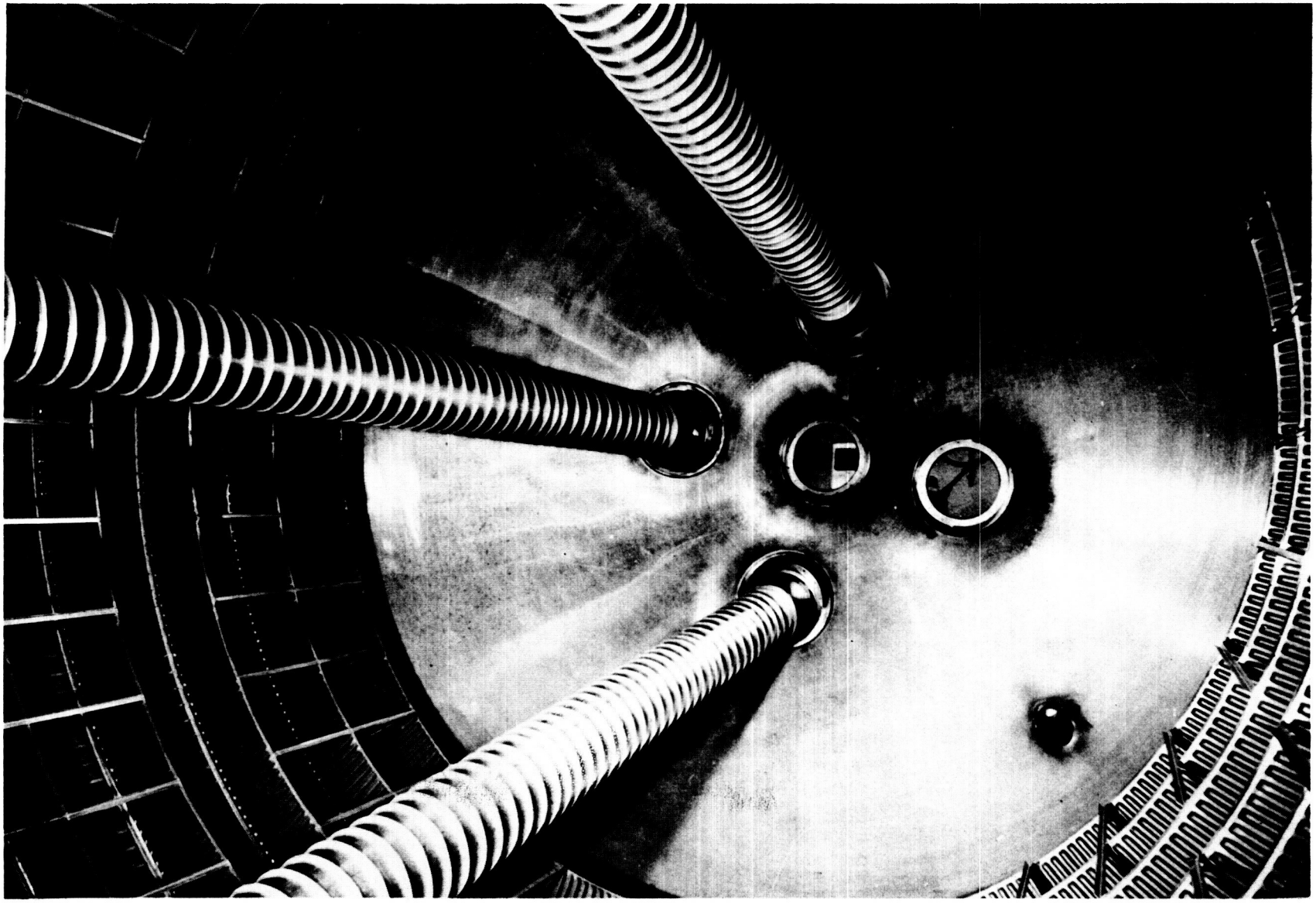

Figure 9.- Internal view of Saturn V model fuel tank.

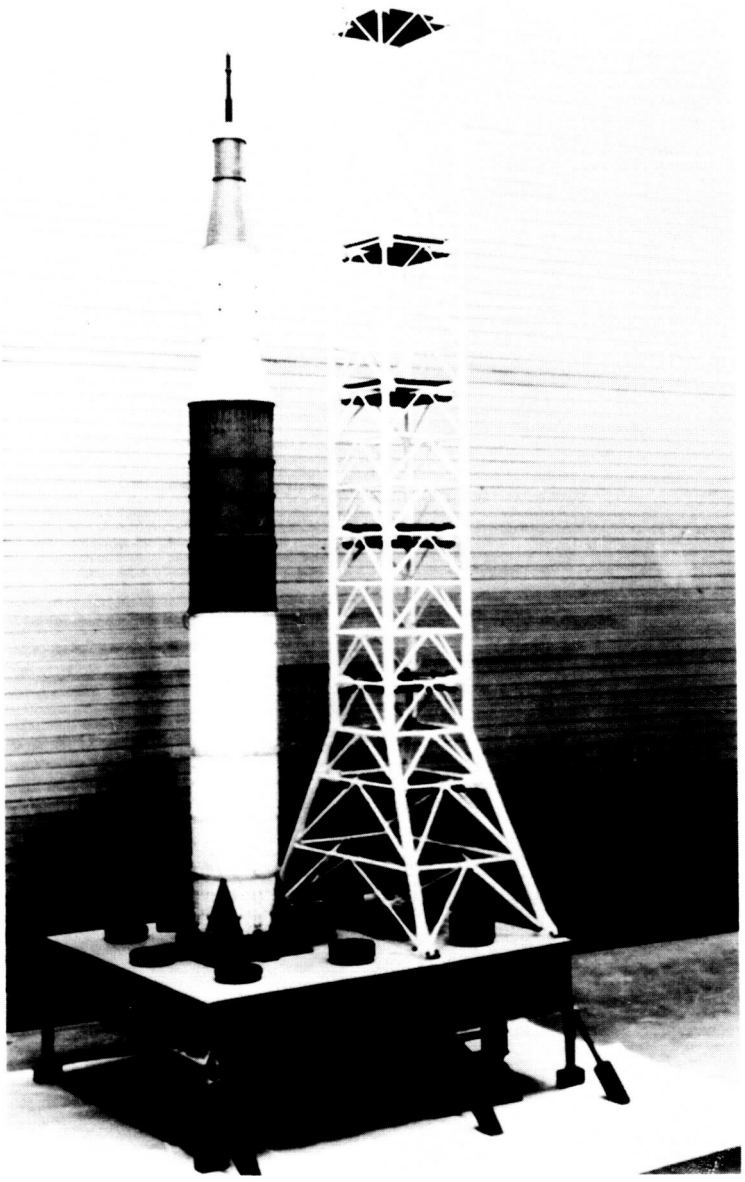

Figure 10.- 1/40-scale model of Saturn V.

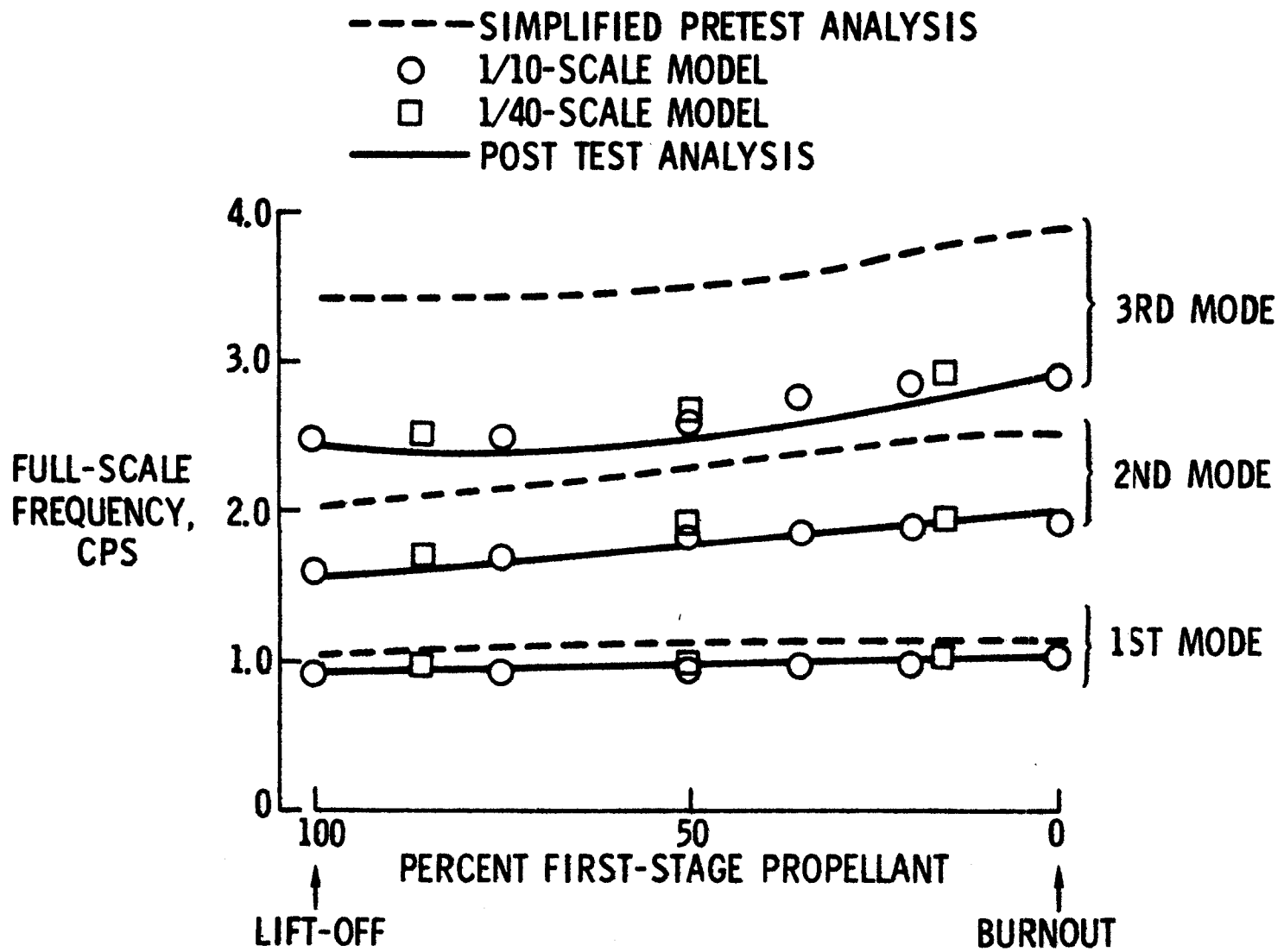

Figure 11.- Lateral bending frequencies of Saturn V models.

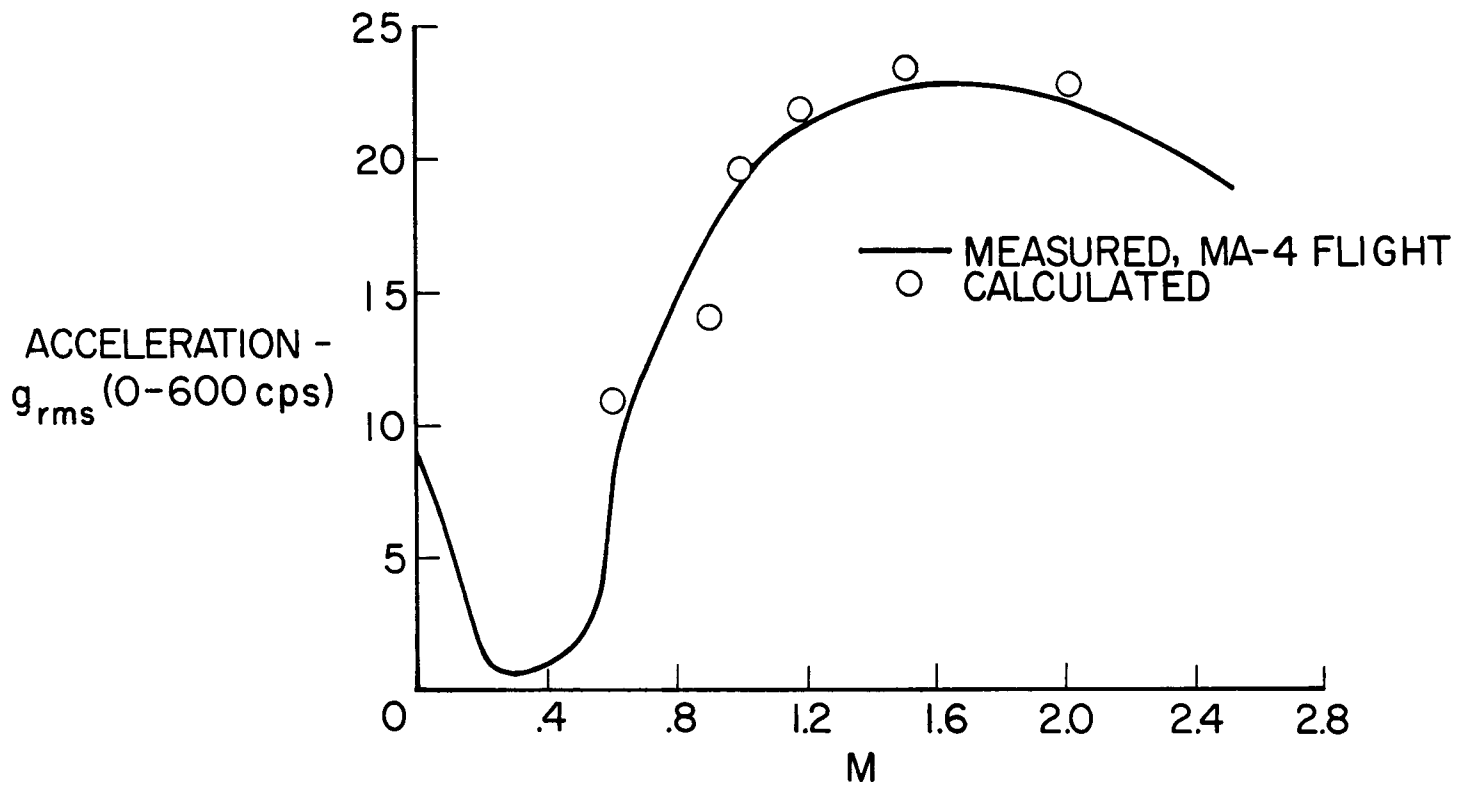

Figure 12.- Comparison of rms acceleration.

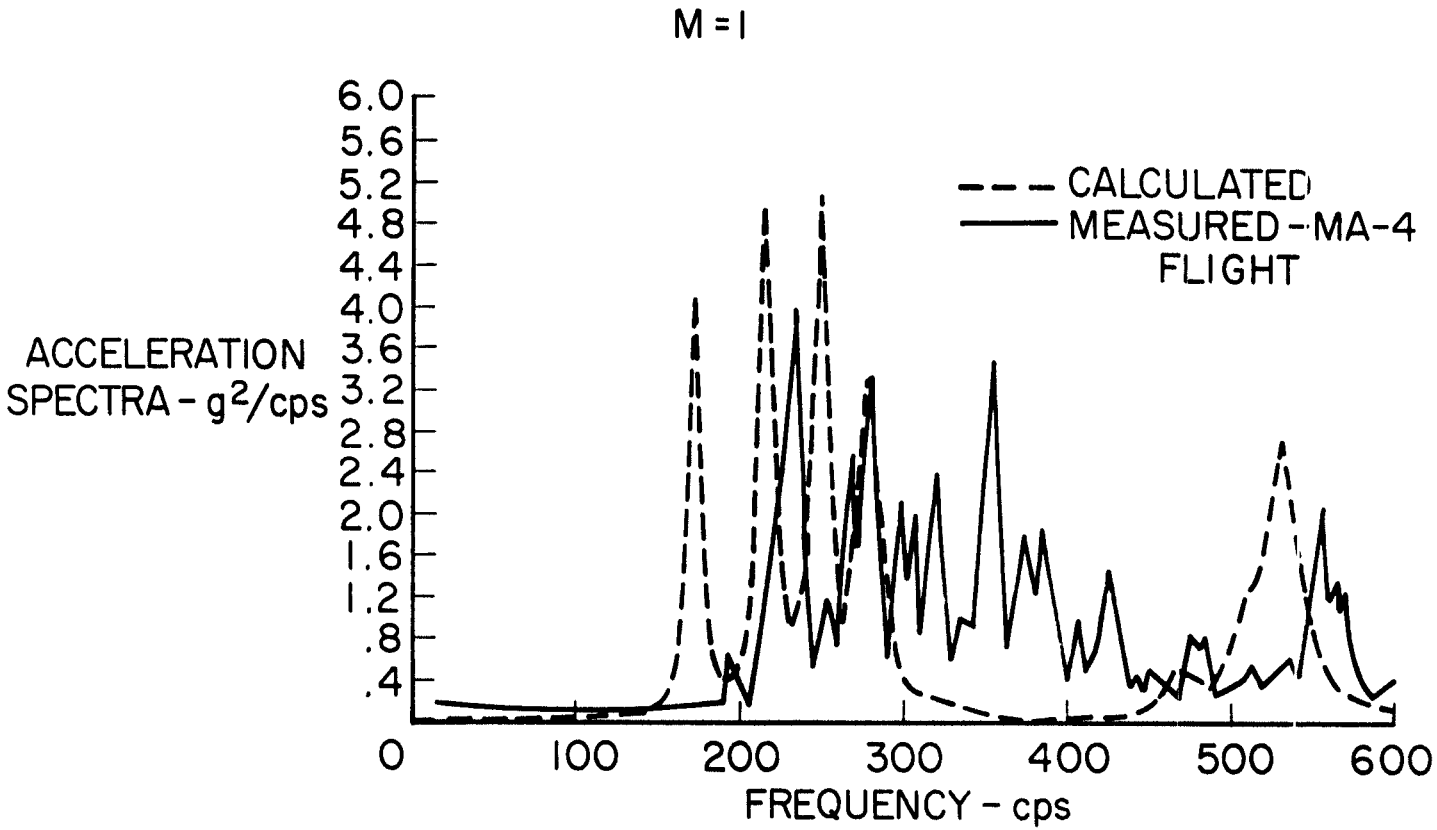

Figure 13.- Acceleration spectra.

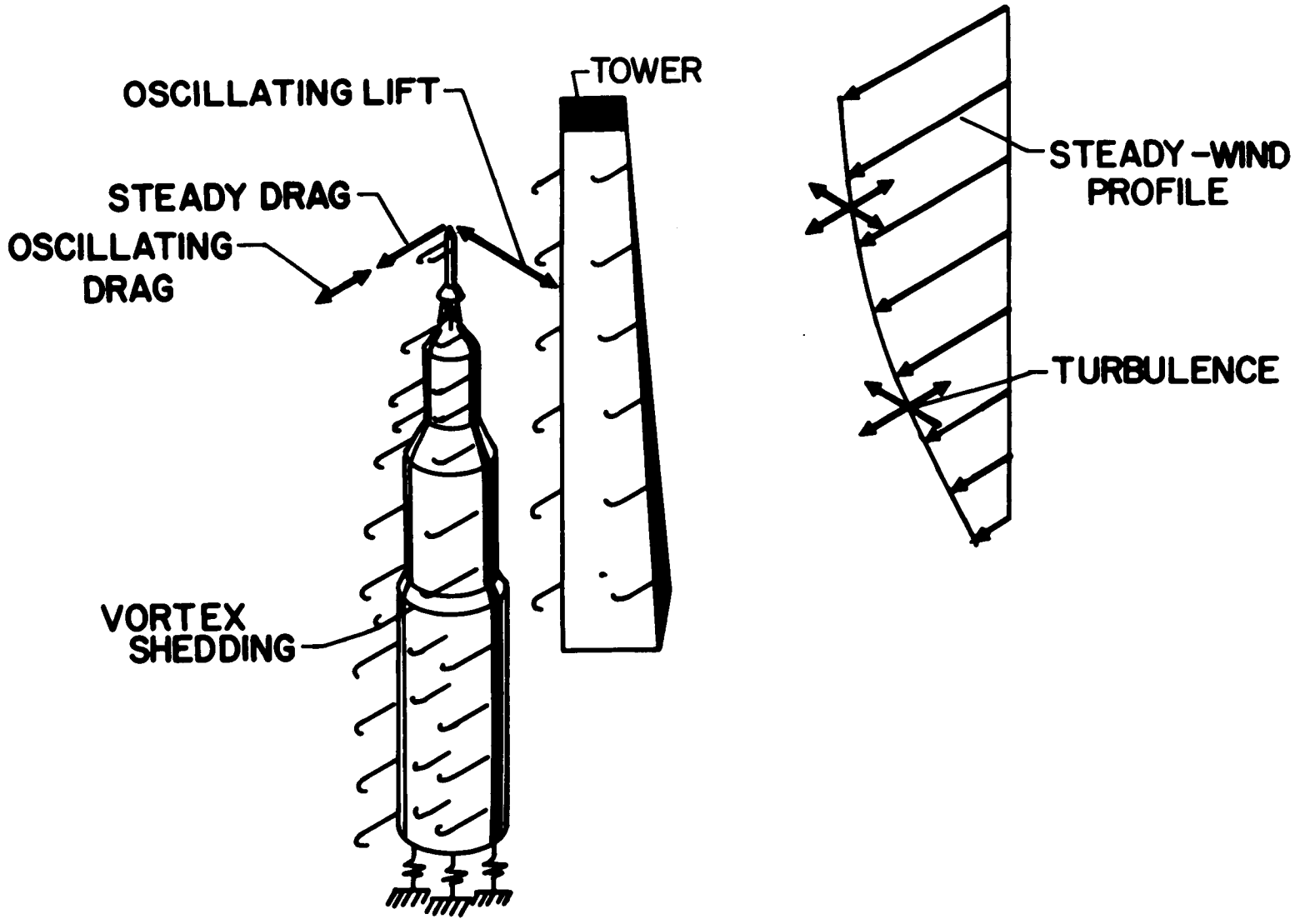

Figure 14.- Load conditions caused by ground winds.

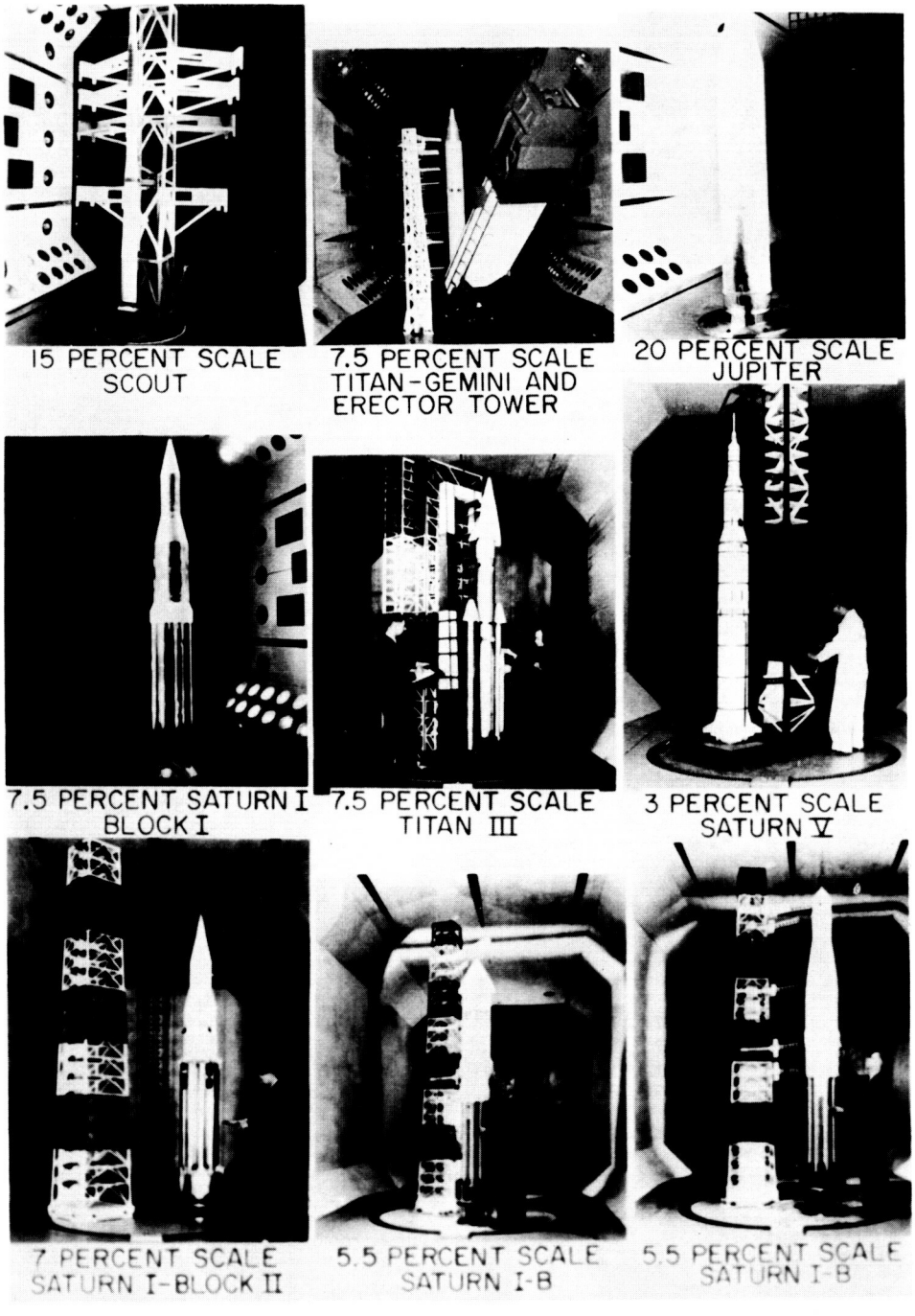

Figure 15.- Some dynamic models used in ground winds research.

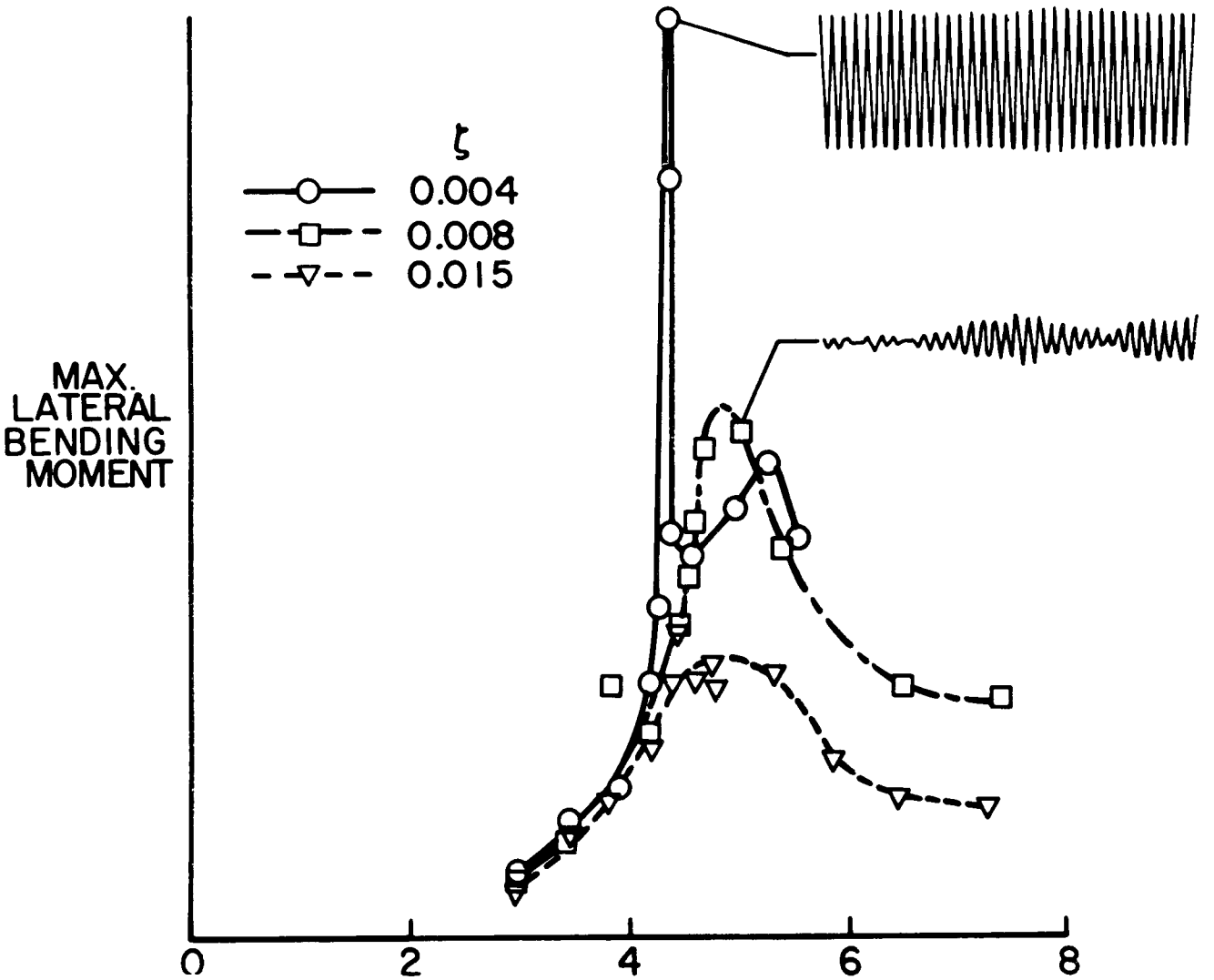

Figure 16.- Effect of damping on Saturn V model response.